Journal of Seismology 2: 337–349, 1998.
© 1998 *Kluwer Academic Publishers. Printed in the Netherlands.*

The Patras earthquake (14 July 1993): relative roles of source, path and site effects

V. Plicka[1], E. Sokos[2], G.-A. Tselentis[2] & J. Zahradník[1]

[1] *Department of Geophysics, Faculty of Mathematics and Physics, Charles University, V Holesovickach 2, 180 00 Prague 8, Czech Republic, e-mail: Vladimir.Plicka@mff.cuni.cz*

[2] *Seismological Laboratory, Section of Applied Geology and Geophysics, Geology Department, University of Patras, Rio 26110, Greece, e-mail: thimios@geology.upatras.gr*

Received 1 August 1997; accepted in revised form 11 September 1998

Key words: crustal propagation, Discrete Wavenumber, Empirical Green's Function, rupture propagation, seismic source, site effects, strong motion modelling

Abstract

A damaging earthquake occurred on 14 July 1993 in Patras, Western Greece. The mainshock (local magnitude 5.1) was followed on the same day by two aftershocks of magnitudes 4.4 M_L and 3.6 M_L, respectively. The strong motion record of the mainshock is studied, based on the teleseismically determined seismic moment and focal mechanism. The Discrete Wavenumber (DW) and Empirical Green's Function (EGF) methods are used. The main conclusion is that the 1993 Patras mainshock had a complex S-wave group mainly due to structural (path and site) effect. However, some effects of the rupture stopping on the peak ground acceleration (0.2 g in the so-called S3 phase) cannot be ruled out. Two values of the source radius are suggested: $R = 1.9$ and 3.0 km. The strong motion record better agrees with $R = 1.9$ km. If the latter is true, the stress drop was of the order of 20 MPa, i.e., higher than often reported for comparable events in Western Greece. Regardless of the true source radius, the ratio of stress drops between the mainshock and aftershocks was about 1–2. The aftershock waveforms indicate significant lateral heterogeneities around Patras. Therefore, the ground-motion predictions of strong events in the area will remain highly non-unique until weak events from an immediate neighbourhood of the particular fault are recorded.

Introduction

A damaging earthquake occurred on 14 July 1993 in Patras, Western Greece. The mainshock (5.1 M_L, Athens magnitude) was followed on the same day by two aftershocks of magnitude 4.4 M_L, and 3.6 M_L. The sequence was recorded in Patras by one of the strong motion stations of the National Observatory of Athens, NOA (Figure 1) (Kalogeras and Stavrakakis, 1995; Stavrakakis et al., 1994). The epicentre location has been determined by several institutes and the most reliable one is that of the local network of the Patras University (PATNET). The mainshock was also recorded by teleseismic stations, thus, the scalar moment, source duration, and focal mechanism have been reported by USGS. As the mainshock had maximum acceleration of 0.2 g at the NOA station and even 0.4 g at a nearby station of ITSAK (ITSAK, 1997), and as it caused damage in the Patras area, it definitely belongs to events important for the future Patras seismic scenario (Tselentis et al., 1996). Therefore, the objective of this paper is to suggest a possible explanation for the NOA strong motion record of the mainshock, consistent with major teleseismic focal data, and some properties of the aftershocks. In particular we are interested in the assessment of relative roles of the source, path and site effects during the studied earthquake.

The innovative features of our study include: (i) a combination of the (point- and finite-source) numerical modelling with the empirical ground motion modelling, and (ii) the empirical modelling treated as an inverse problem with two independent unknowns, the mainshock source radius, and the mainshock/aftershock stress-drop ratio.

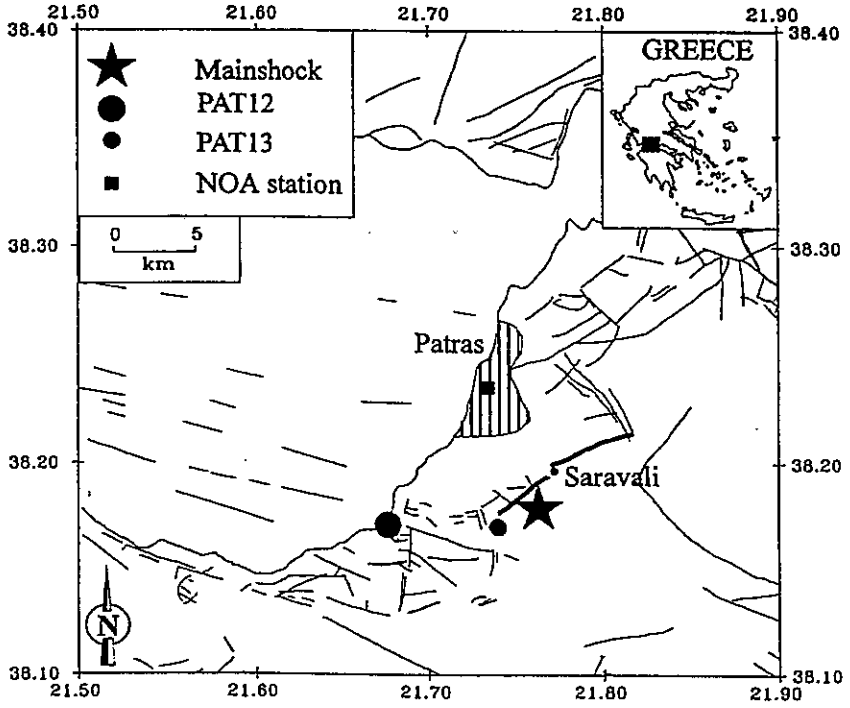

Figure 1. Map showing epicentre location of the three events under study with respect to NOA strong motion recording site, town of Patras and neotectonic faults at the area.

Data

Epicentres of the studied events (Figure 1), determined by PATNET, have accuracy of about 0.5 km. The focal depths are less reliable, but are most likely around 5 km. The globally determined parameters (USGS, 1993) of the mainshock include: seismic moment $M_0 = 3.2{*}10^{17}$ Nm, and focal mechanism given by the fault plane with strike 238°, dip 73°, and rake −163°.

The records studied in this paper are PAT11 (mainshock) and PAT12 and PAT13 (4.4 M_L and 3.6 M_L aftershocks), taken from Kalogeras and Stavrakakis (1995); Figure 2. Those records are SMA-1 analog records, corrected for instrumental effect and digitisation errors, hence providing true ground motion in the frequency band from $f1$ to 25 Hz, where $f1 = 0.25$, 0.5, and 0.7 Hz for PAT11, 12, and 13, respectively.

The crustal structure of Western Greece is roughly known (Makris, 1977; Panagiotopoulos and Papazachos, 1985; Pedotti, 1988; Melis et al., 1989), see model M1 in Table 1. Due to its simplicity, this model could not explain the arrival times of the main phases of the NOA mainshock record. Therefore, the arrival times of the P wave (assumed to be at the triggering time), SP wave and direct S wave (assumed to be at the beginning of the strong S-wave group) were used to modify the crustal model in its upper part by the ray method (Zednik et al., 1993). The modified model

Table 1. The original crustal model M1 of Western Greece

Depth (km)	Vp (km s^{-1})	Vs (km s^{-1})	ρ (kg m^{-3})
0	5.70	3.20	2840
5	6.00	3.37	2900
18	6.40	3.60	2980
39	7.90	4.44	3280

Table 2. The modified crustal model MN3 of Western Greece

Depth (km)	Vp (km s^{-1})	Vs (km s^{-1})	ρ (kg m^{-3})
0	1.42	0.21	2500
0.05	2.67	0.56	2500
1	4.45	2.50	2500
2	5.70	3.20	2840
5	6.00	3.37	2900
18	6.40	3.60	2980
39	7.90	4.40	3280

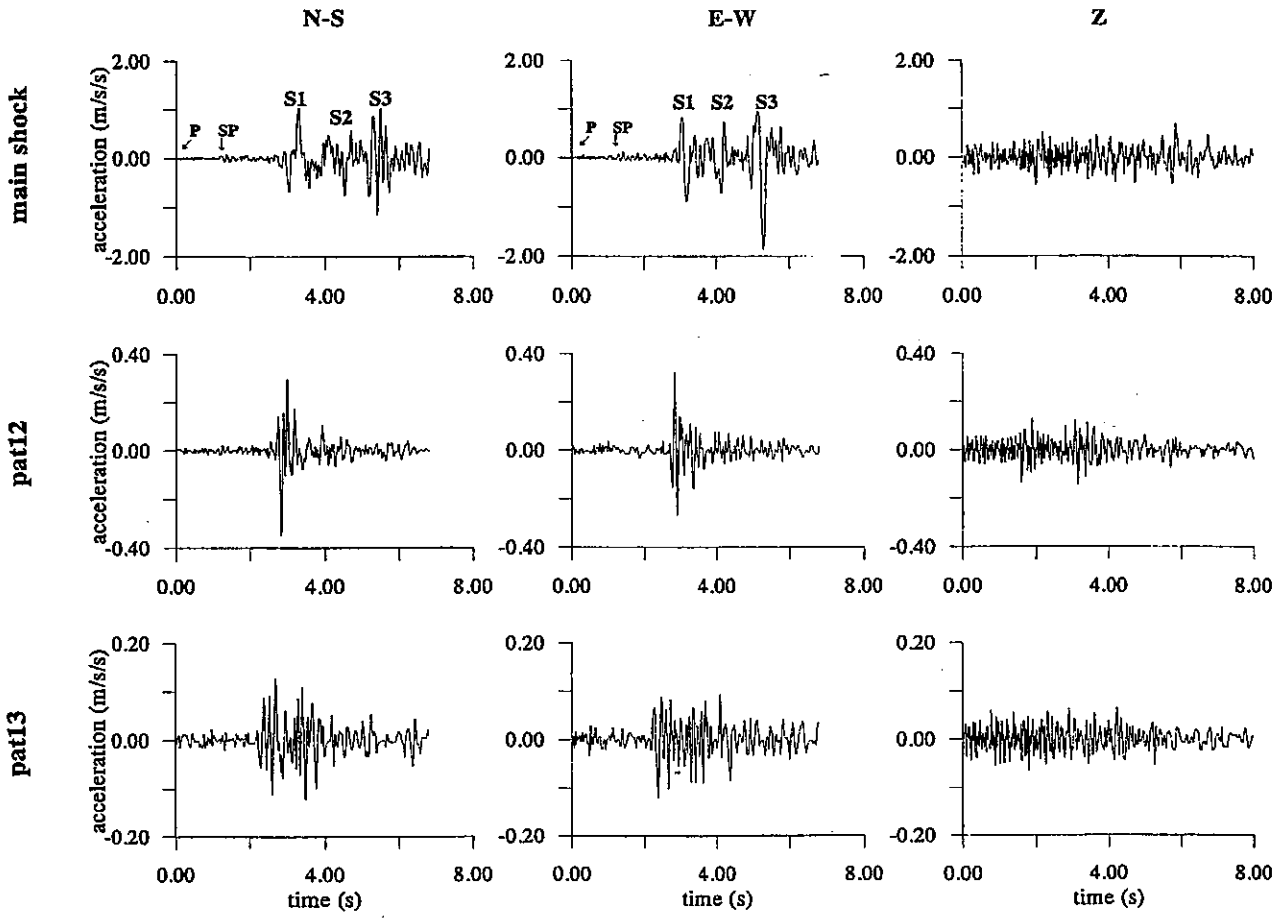

Figure 2. Acceleration records of the mainshock and the two aftershocks at the NOA station in Patras.

MN3, given in Table 2, has been obtained for the assumed hypocentral depth of 5 km. The model features a high velocity ratio $\frac{V_p}{V_s} = 4.76$ in the upper 1 km, and in particular a very high ratio $\frac{V_p}{V_s} = 6.76$ in the top 50 m.

This high $\frac{V_p}{V_s}$ ratio, necessary to fit the P, SP, and S arrival times, is consistent with geophysical measurements close to the NOA station (Koukis et al., 1997). In this sense the top 50 m layer represents our site model. Although the available data are not complete enough to allow a detailed analysis of site effects close to the NOA station, preliminary calculations by the finite-difference method did not reveal major lateral wave propagation effects there (Tselentis et al., 1996).

Focal mechanisms of the aftershocks are not available. A visual inspection of the NOA records indicates that most likely both PAT12 and PAT13 had a large S/P amplitude ratio, thus indicating similarity with the mainshock, for which NOA is close to the P-wave nodal plane. From the S/SP amplitude ratios it seems that the focal mechanism of PAT13 was closer to that of the mainshock than the one of PAT12. Also the location of PAT13 is closer to the mainshock.

The two aftershocks not only differ from each other by their S/SP amplitude ratios, but also the duration of their S wave groups is different. As PAT12 is a more distant event than PAT13, the PAT12 duration is expected to be longer. Because the opposite has been observed in the records, it is inferred that the S-wave group duration is a feature sensitive to local structure variations along different source-receiver paths in the Patras region.

A prominent feature of the NOA record is the complexity of the S-wave group, marked by three major arrivals, S1, S2, and S3 (Figure 2). This denotation was introduced in a previous publication (Tselentis et al., 1996) when analysing the Patras'93 mainshock at two stations close to NOA, the so-called stations B and C of ITSAK (Figure 3). The two stations recorded

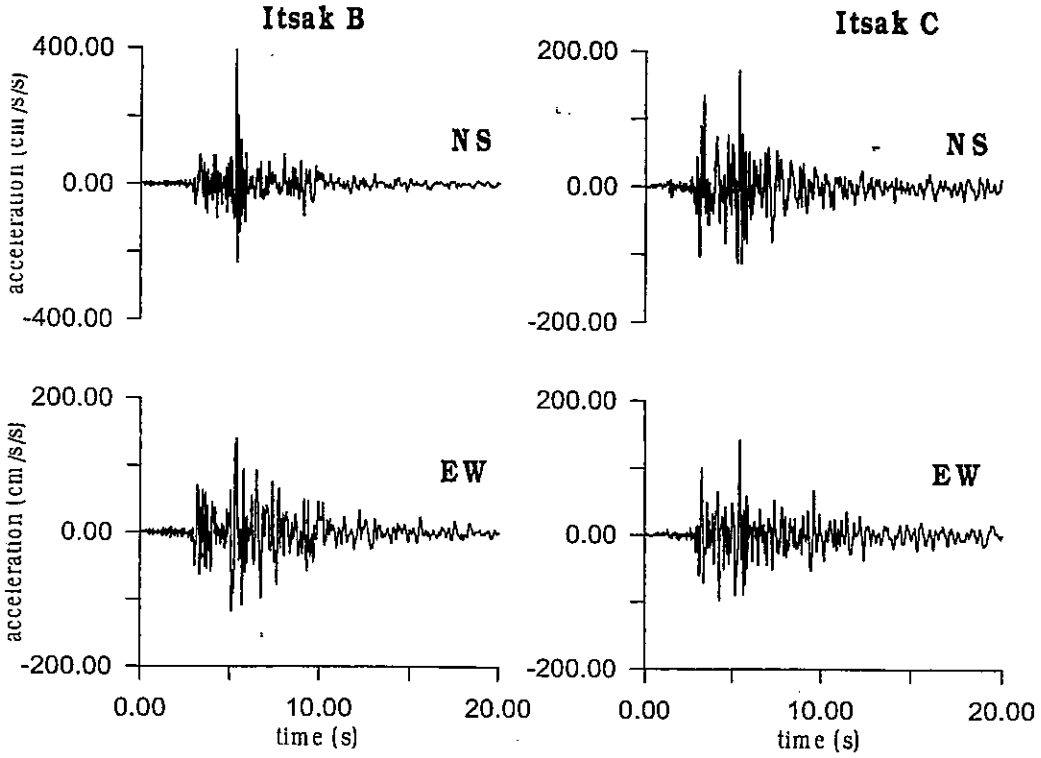

Figure 3. The mainshock acceleration time histories recorded at sites B and C of ITSAK in Patras. Note a different scale of the top left panel.

peak accelerations of 0.4 and 0.2 g, respectively. Insufficient data did not allow us to explain this amplitude difference by numerical modelling. Other local events simultaneously recorded at the two ITSAK stations did not confirm stable differences between B and C, hence excluded simple explanations in terms of pure site effects. That is why in the present study we do not deal anymore with the differences between the stations, but rather concentrate on their common features, i.e., just the *presence* of the two most prominent phases S1, and S3. In particular, we try to understand, how the source, path and site effect contributed to these phases during the mainshock at the NOA station.

Methods used to explain the NOA mainshock record

Our analysis of the NOA mainshock record PAT11 is based mainly on the teleseismic estimates of the seismic moment and focal mechanism, the NOA record of the PAT13 aftershock, and the numerical modelling of PAT11 by two methods. They are the Discrete-Wavenumber (DW) method of Bouchon (1981) and Coutant (1989), and the Empirical Green's Function (EGF) method of Irikura and Kamae (1994). The main parameter of interest is the fault size ('radius'), related to the stress-drop, and having important tectonophysical consequences.

Experiment 1 – point source modelling

In this experiment we use the teleseismic estimate of source duration $T = 3.2$ s (USGS, 1993). That value, taken from Harvard CMT catalogue, is not determined from the inversion of data for a particular earthquake, but from empirical formula (Ekström, 1992) equivalent to a constant stress drop. As such, the value of $T = 3.2$ s does not represent any firm constraint of the Patras event since the true duration may deviate from this empirical estimate. Thus, as a first approximation, we estimate the source radius to be of $R = 3$ km. This, together with the seismic moment, yields the stress drop of $\Delta\sigma = 5$ MPa. The latter agrees with values so far reported in Western Greece for comparable events (Melis et al., 1995; Stavrakakis et al., 1994).

Now we produce the point-source synthetics for the NOA station by the DW method. The trapezoidal time function is used, with duration varied around

$T = 3$ s. The crustal structure is that of model MN3. We filter out the very low and high frequencies in the same way as made during the digitization. The best agreement between the synthetic and real acceleration records, Figure 4a, was obtained for a slightly asymmetrical trapezoidal source time function, 2.5 s long. The synthetics exhibit the S1 and S3 phases quite well, even with reasonable amplitudes in the case when the velocity model is supplemented by Q values as low as 10 and 50 in the upper 50 m and 1000 m thick layers respectively, while having $Q = 300$ in the deeper layers.

A similar experiment was also repeated for Brune's pulse, but in this case the synthetics did not explain the S3 phase at all (Figure 4b). It suggests that the S3 phase could be a stopping phase, well modelled by the rear part of the trapezoid, but too poor in the Brune pulse due to its smooth decay.

Experiment 2 – EGF modelling

Although Experiment 1 provided a possible explanation of the mainshock (a surprisingly good result if we take into account that the acceleration history was modelled purely theoretically), an alternative explanation should obviously also be looked for. Not only because the problem is non-unique, but also because the other possible explanation may be physically quite different. In particular, we want to explore if a more realistical path description and a simple rupture scenario of a finite fault would again require the source radius of about 3 km. To this goal we perform the EGF modelling of the NOA mainshock record, using the PAT13 aftershock as a subevent. The criterion is again the agreement between the synthetic and NOA records, in particular the fit to the S-wave group.

The path and site effects are represented by the weak event, i.e., without any need of the structural model. The low- and high-frequency filtering, typical for the NOA records, is applied (with the cosine tapers 0.2–0.25 and 0.4–0.7 Hz for the mainshock and the aftershock, respectively, and 25–27 Hz for both). Although the focal mechanism of PAT13 weak event may have been similar to the mainshock we do not study it in more detail, because the a priori proof of the focal-mechanism similarity is not required in our modelling. This is because we are using the EGF method neither for the strong-motion prediction, nor for the deconvolution of the mainshock time-function. Instead, we are employing the EGF method in the inverse problem whose main target is to fit the S1 and S3 wave groups by varying (mainly) the source radius. In such a situation we have three possibilities: (i) The aftershock and mainshock mechanisms are in relatively good agreement, then we reach the fit and estimate the radius, or, (ii) the focal mechanism effect is less affecting the observed record than the structural effect, and we again reach the fit even with a less good subfault focal mechanism, or, (iii) we do not get the fit (e.g., the synthetic S-wave group is too short), it does not matter whether due to a bad mechanism or a bad path description, and then we stop drawing any further conclusion about the source radius. As shown below, it seems that our case was somewhere between (i) and (ii). Another reason for not considering the focal mechanism in greater detail is that the EGF synthesis of finite faults can not fully account for the radiation differences of the individual subfaults. The accurate focal mechanism treatment would require the so-called EGTD method (Plicka and Zahradnik, 1998) which is much beyond the scope of this paper.

The experiment assumes a rupture in the plane having the mainshock strike and dip, that propagates radially from the hypocenter at constant speed (we take 2.6 km s^{-1}, which is 81% of the shear-wave velocity at the hypocenter, and resulted from trials between 2.5 and 2.9 km s^{-1}). The radial rupture propagation has been adopted because of its simplicity that eliminates the need of additional rupture parameters.

We adopt the teleseismic moment of the mainshock, $M_0 = 3.2 * 10^{17}$ Nm. Using empirical relations between moment and local magnitude (Melis et al., 1995), we estimate the aftershock moment as $m_0 = \frac{M_0}{500}$. We do not assume anything else about the weak event, due to uncertainties connected with the estimation of its source radius r and stress-drop $\Delta\sigma_a$. Then we have four unknowns, $R, r, \Delta\sigma, \Delta\sigma_a$, connected by two relations: $(M_0/cm_0) = (R/r)^3$, and $c = \Delta\sigma/\Delta\sigma_a$, from which we can select two free parameters for the inversion. We selected the source radius of the mainshock R, and the ratio of the stress drops $c = \Delta\sigma/\Delta\sigma_a$. For each observation a prediction error was defined, $e_i = d_i^{\text{obs}} - d_i^{\text{pre}}$ (Menke, 1984), where d_i is the amplitude of the i-th sample of the time series, $i = 1, 2, \ldots, N$. The best fit is then the one with model parameters that lead to the smallest overall error E, defined as $E = \sum_{i=1}^{N} e_i^2$. The systematic search is used, with 4000 tested combinations.

The best-fitting synthetics, Figure 5, were obtained for $R = 1.9$ km, and $c = 2$ (error $E = 215.6$), and reproduce the S1 and S3 phases quite well. Of

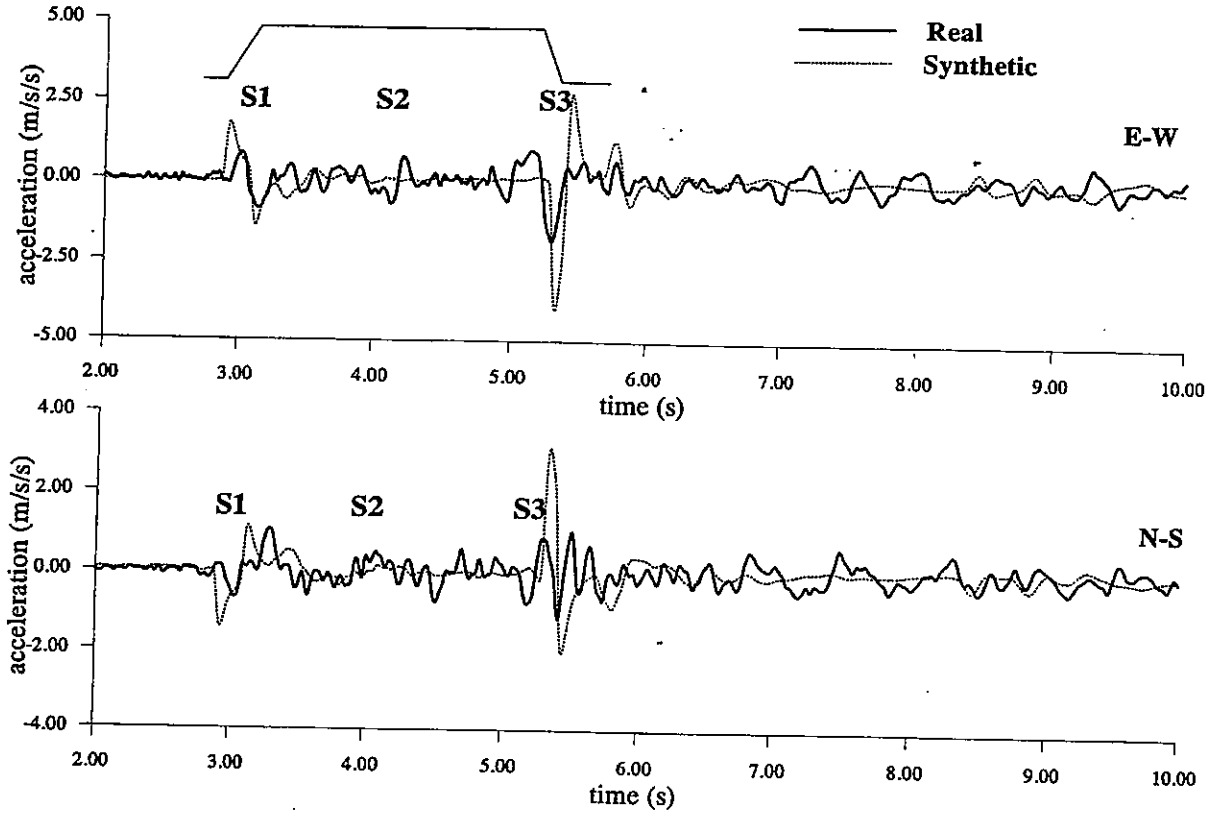

Figure 4a. Comparison between observed and synthetic strong-motion acceleration time histories of the mainshock. The synthetics were produced by the DW method, employing a *point source* of the *trapezoidal* time function.

course, the so-called 'good fit' is to be understood in the same sense as in the other strong motion studies (Diagourtas et al., 1994; Hutchings, 1994; Irikura and Kamae, 1994), i.e., we focus on the presence of the wave groups, their shape, and their relative amplitudes, rather than on all individual waveform details.

Anyway, to consider the possibility of a larger source as well, indicated by Experiment 1, we also artificially constrained the radius to be $R = 3$ km. In this case the only free parameter was c, and the search resulted in $c = 1$ (error $E = 325.7$). Although worse than in the previous case of $R = 1.9$ km, the agreement between the synthetic and observed S-wave group is acceptable (Figure 6).

When trying to understand why the simple summation provided the explanation we have to bear in mind that although a single weak event (PAT13) was used in the EGF synthesis, the variability of the path effect between individual subfaults and the station was at least approximately accounted for by the time shifts and amplitude scaling (Equation 2.6 of Irikura and Kamae, 1994).

Similar experiments done with the PAT12 aftershock provided a much worse fit, i.e., a too simple synthetic S-wave group, the S3 pulse being absent. The failure of PAT12 aftershock is most likely due to its location, too far from the mainshock epicentre, thus disabling a correct path representation.

Experiment 3 – EGF and finite-source DW modelling

This is again Irikura's summation, in which, however, instead of the PAT13 aftershock a *synthetic* weak event calculated by the DW method is employed.

A weak event at the NOA station was arbitrarily modelled as a point source of moment $m_0 = 1.5 * 10^{14}$ Nm, with a Brune's pulse, and a corner frequency of 3.8 Hz. The source was embedded in model MN3 ($Q = 300$ everywhere), and having exactly the same hypocenter and focal mechanism as that of the main-

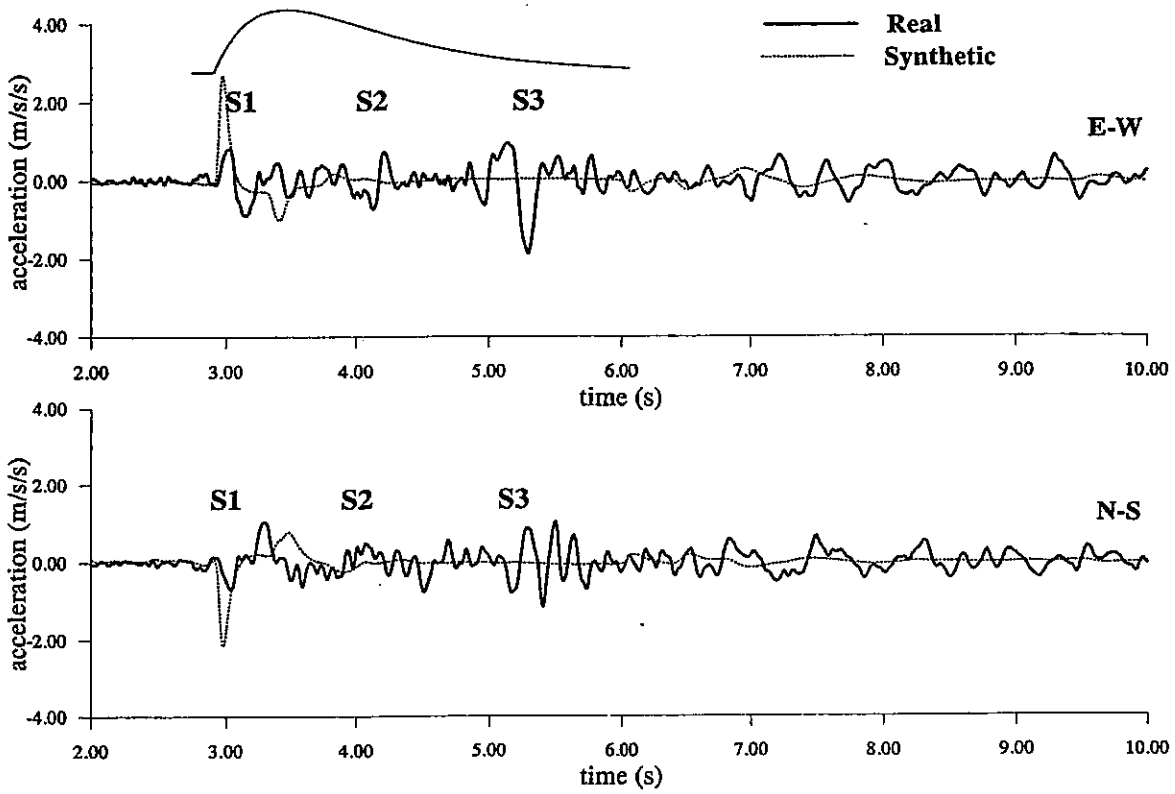

Figure 4b. Comparison between observed and synthetic strong-motion acceleration time histories of the mainshock. The synthetics were produced by the DW method, employing a *point source* of the *Brune* time function.

shock. The trapezoidal impulse provided analogous results, too. The synthetic weak event is compared with the PAT13 record in Figure 7. The summation is identical to that of Experiment 2. The best fitting synthetic record is shown in Figure 8. In contrast to Experiment 2, the agreement is much worse, not representing the S3 phase at all.

Our interpretation of the results is as follows: Experiment 3 kept the summation of Experiment 2, i.e., it modelled the same, relatively smooth rupture history. This was combined with the DW path modelling, representing an 'impulse response of the medium', like the one used in Experiment 1. Although Experiments 1 and 2 were successful, the latter combination of a relatively smooth source time function and a relatively short DW impulse response in Experiment 3 does not satisfy the NOA mainshock record. This indicates the insufficiency of model MN3. The same negative result was obtained for other parameters of the DW-synthesized weak event, used to sum up the mainshock, although the weak end strong events had the same focal mechanisms.

Similar experiments were also performed with several sources of finite extent (dislocation and quasidynamic ones), embedded in model MN3, *completely* modelled by the DW method. The source size was taken from Experiment 2 ($R = 1.9$ km and 3.0 km), the rupture propagated radially from the hypocentre at a constant speed of 2.6 km s^{-1}. The fault plane was subdivided into 128 and 317 subsources, with their radii of 300 m and 320 m, respectively. When requiring two or more subsources per wavelength the summation is coherent up to about 5 Hz. Higher frequencies were filtered out from both the synthetic and real record (see Figure 9). Although Green's functions from all subsources were fully considered, negative results similar to those of Figure 8 were obtained, featuring a too short synthesized S-wave group, with a single dominant pulse only.

The same conclusions were found also from Experiment 3 repeated for the velocity modelling. In spite of the fact that the velocity records were simpler than the acceleration ones, the attempts to explain the presence of S3 wave group were not successful.

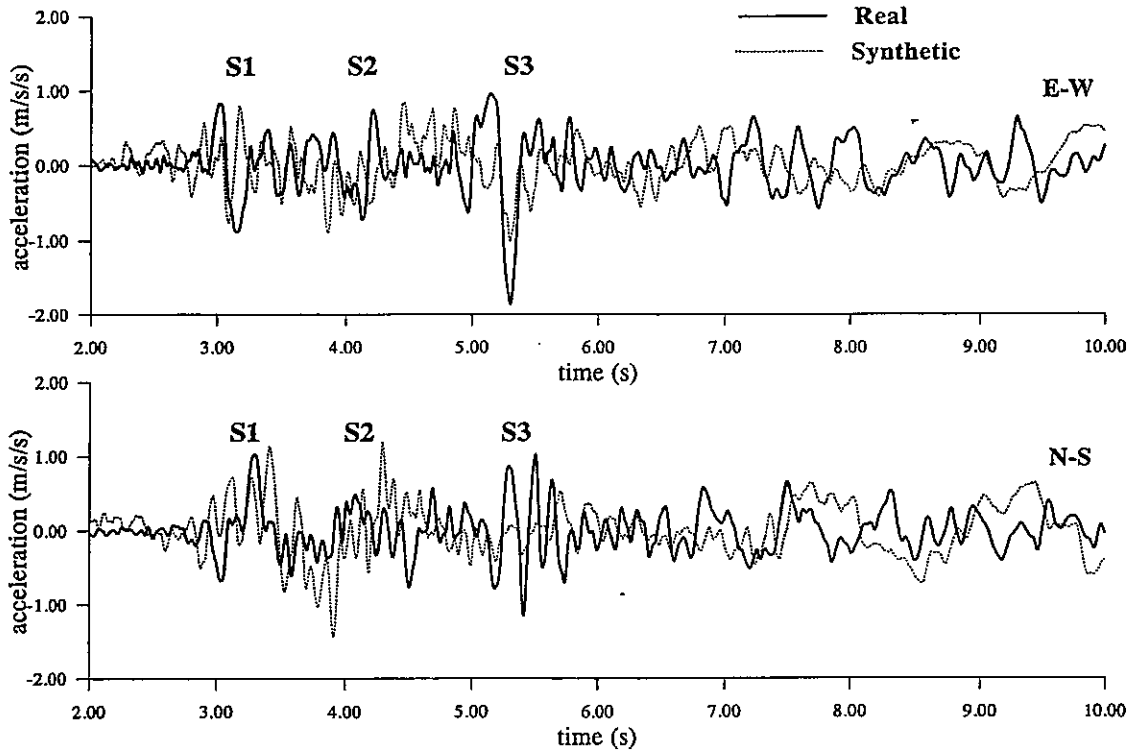

Figure 5. Comparison between observed and synthetic strong-motion acceleration time histories of the mainshock. The synthetics were produced by the EGF method, employing PAT13 aftershock as subevents, and having *source radius of* $R = 1.9$ km.

The main conclusion from the finite-extent DW modelling is that even $R = 3$ km is not large enough when explaining the S1–S3 wave group. This is due to simplicity of the Green function, and partly also due to narrowing of the apparent source time function for the NOA station by the directivity effect. It indicates that S1–S3 group should be explained as a combined source and path effect in a structure more complex than model MN3. That was just the case of the EGF simulation in Experiment 2, where the employment of the realistic path description allowed for $R = 3$ km, but permitted even smaller radii, e.g., $R = 1.9$ km.

Discussion

Let us analyse, in the light of the previous experiments, what were the successful combinations of the source and path descriptions used in Experiment 1 and 2. Experiment 1, although using the short DW impulse response of the medium in model MN3, was successful due to its dramatic rupture stopping, modelled by the trapezoid. On the other hand, Experiment 2, though equivalent to a smooth time function, was successful due to its relatively long duration and complexity of the structural response represented by the PAT13 aftershock.

The source radius of $R = 1.9$ km and $c = 2$ was identified as the best in Experiment 2, but $R = 3$ km and $c = 1$ was also acceptable. Then Experiment 3 showed that structural model MN3 is too simple. Therefore, from two successful explanations of the NOA record in Experiment 1 and 2 the one of Experiment 2, independent of model MN3, seems more likely.

In other words, the complex S-wave group was probably due to the considerably complicated (long) response of the medium. By medium we mean the crustal structure including its top low-velocity layers, hence, to some extent, also the site effect. The S3 phase may have been produced by a combination of the structural and source (stopping) effect.

In this sense our discussion is similar to that of Stavrakakis et al. (1994), who, however, did not

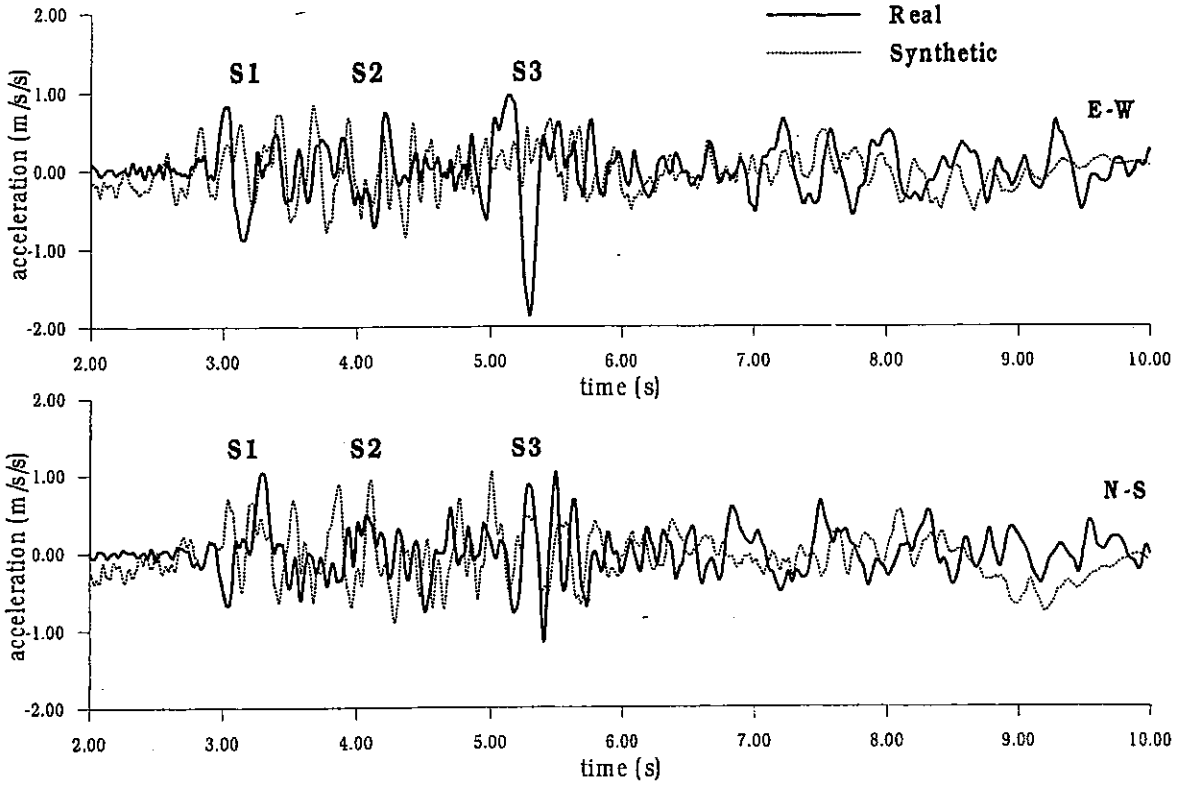

Figure 6. Comparison between observed and synthetic strong-motion acceleration time histories of the mainshock. The synthetics were produced by the EGF method, employing PAT13 aftershock as subevents, and having *source radius of* $R = 3$ km.

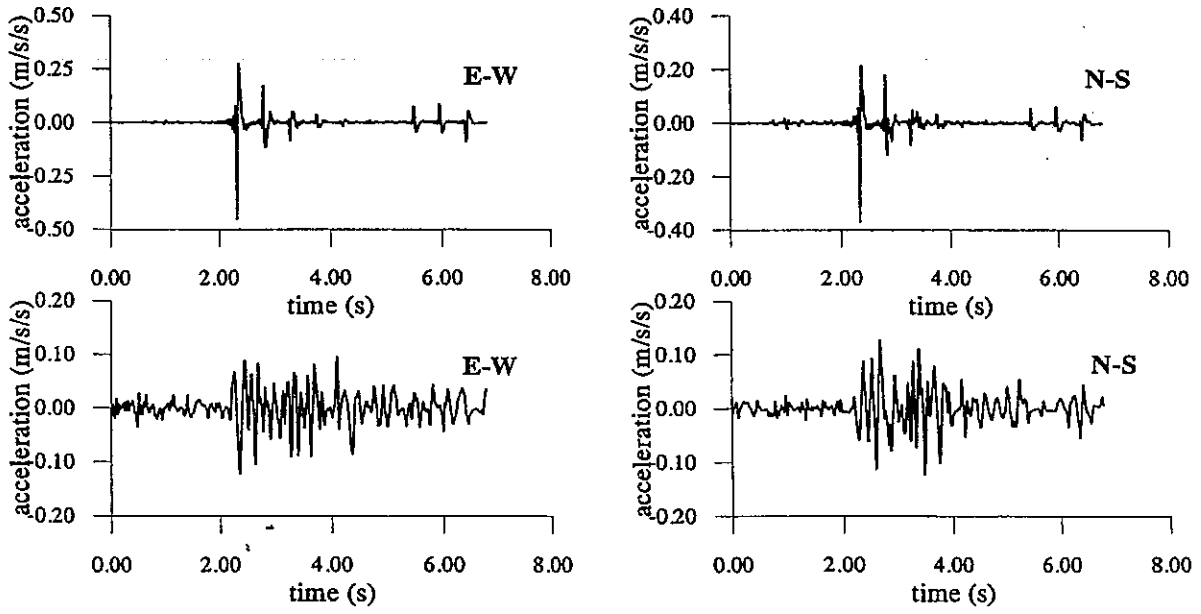

Figure 7. Comparison between synthetic (top) and real (bottom) weak-event records. The synthetics were produced by the DW method, while the real record is PAT13 aftershock.

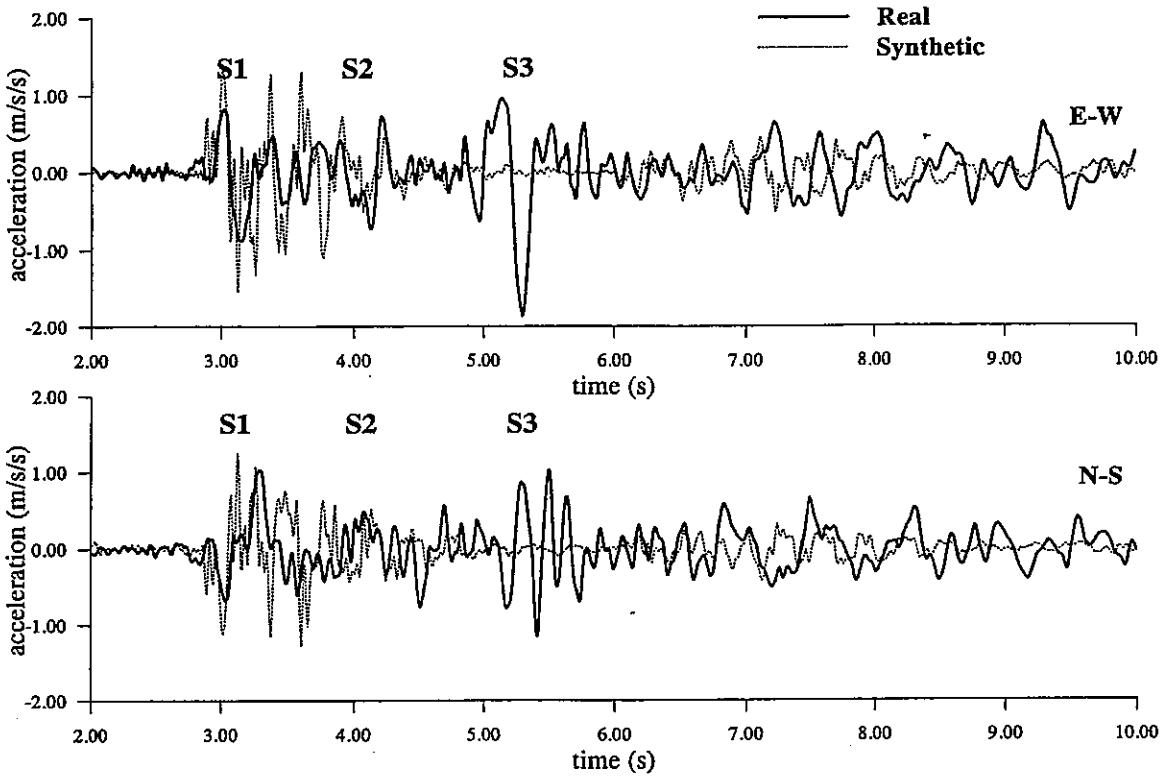

Figure 8. Comparison between observed and synthetic strong-motion acceleration time histories of the mainshock. The synthetics were produced by the EGF method, employing a *synthetic subevent* calculated by the DW method.

explain the problem by the presence of a complex structure, but attributed it to source complexity.

Two issues deserve more attention, i.e., validating the assumed value of m_0, and checking the value of r that was (implicitly) determined by the EGF modelling. We assumed $m_0 = \frac{M_0}{500}$, and the resulting values of $R = 1.9$ and 3.0 km provided $r = 0.3$ and 0.4 km, respectively. An efficient verification is possible by means of the mainshock/aftershock spectral ratio (Lindley, 1994). At frequencies greater than corner frequency of the aftershock, the ratio of two (presumably Brune omega-squared) spectra should equal to a constant value $c\frac{R}{r}$, that is 13 and 8 for our two solutions, respectively. Indeed, as seen from Figure 10, these values are in agreement with the observed high-frequency limit of the ratio. Thus, we get an a posteriori verification of the employed m_0. Moreover, Figure 10 also shows two mainshock/aftershock theoretical ratios (Equation 1 of Lindley, 1994) corresponding to our $\frac{M_0}{m_0}$, and to our two pairs of R and r. The data, available for $f > 0.7$ Hz, are in an acceptable agreement with these two models. This validates not only $\frac{R}{r}$ (as the high-frequency limit did), but also R and r separately. Again, as in Experiment 2, $R = 1.9$ km seems to be somewhat better than 3.0 km.

Conclusions

The main shock of the Patras sequence of 14 July 1993 recorded by the strong motion NOA station in Patras, was modelled by the Discrete Wavenumber (DW) and Empirical Green's Function (EGF) methods.

Experiment 1 suggested the possibility of a source of radius $R = 3$ km with a relatively abrupt rupture stopping, represented by a trapezoidal time function, that fitted the observed prominent S3 phase quite well (although the considered structural model was simple enough).

From Experiment 2 we learned that the complexity of the S-wave group can be explained as a result of the complex crustal structure.

Experiment 3 showed that model MN3 is not adequate to explain the true structural effect. From such a point of view the success of Experiment 1 (in

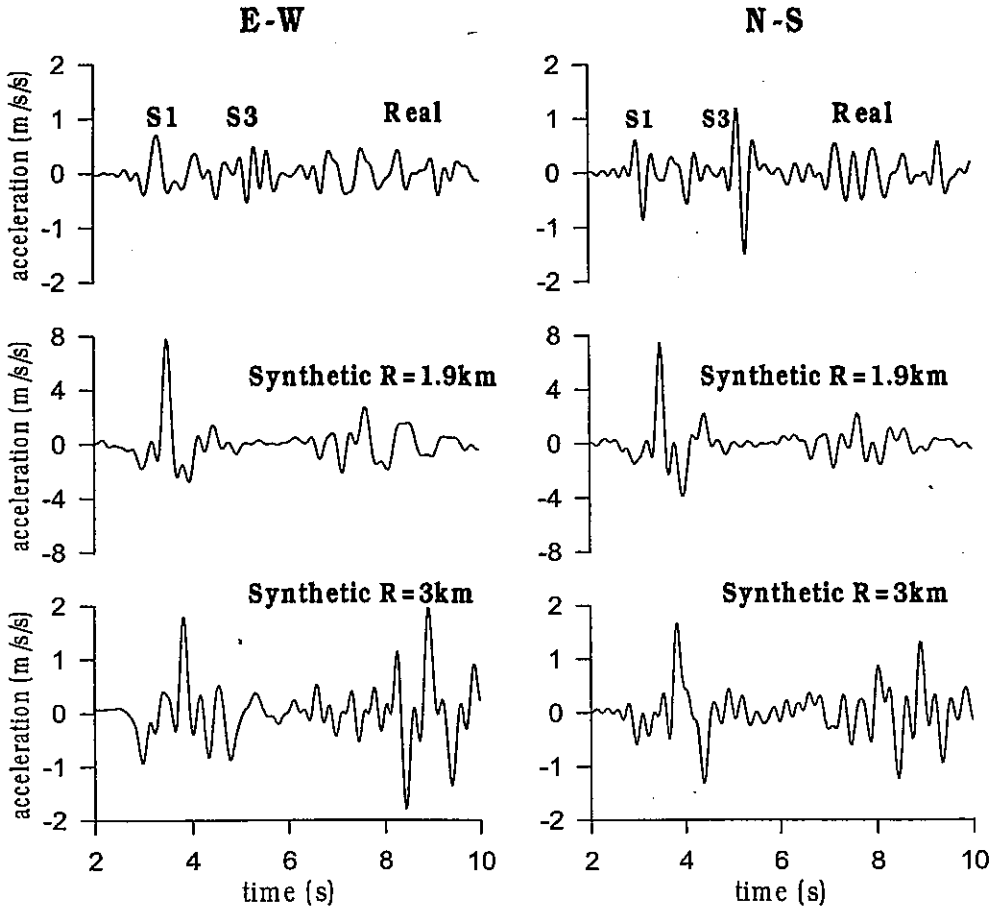

Figure 9. Comparison between observed (top) and synthetic strong-motion acceleration time histories of the mainshock. Frequencies higher than 5 Hz were filtered out. The synthetics were produced by the DW method for a *finite-extent dislocation* source model. The source radii are $R = 1.9$ km (middle), and $R = 3.0$ km (bottom) respectively.

which the model MN3 was also used) seems somewhat artificial. It also demonstrated failures of the DW finite-extent modelling in model MN3, thus proving that the realistic path representation is more critical than the aftershock/mainshock focal-mechanism similarity, and the availability of Green function from many subsources.

Two source radii were suggested by Experiment 2: $R = 1.9$ and 3.0 km. However, $R = 1.9$ km provided better agreement with NOA record. If the latter was true, the stress drop was 20 MPa, i.e., higher than often estimated for Western Greece.

As the EGF modelling in this paper was treated as a two-parameter inverse problem, it resulted also in the evaluation of the mainshock/aftershock stress drop ratio, c. Regardless of the true value of R, the stress drop ratio was $c = 1$ to 2.

It is also concluded that the Patras '93 mainshock had a complex S-wave group mainly due to structural (path and site) effect, although some effects of the rupture stopping on S3 phase cannot be ruled out.

A practical result is that the empirical summation was sensitive to the choice of the weak event (a very bad fit to NOA mainshock was obtained when synthesising the mainshock from PAT12, instead of PAT13 aftershock). This means that the Patras area includes significant lateral heterogeneities. Therefore, the scenario predictions for a particular fault in Patras area require weak event recordings just from foci in vicinity of the expected strong shock. In other words, a general strong motion prediction (that from an arbitrary fault) is highly nonunique in the Patras area.

A by-product of the identified structural complexity is that without a better knowledge of the near-

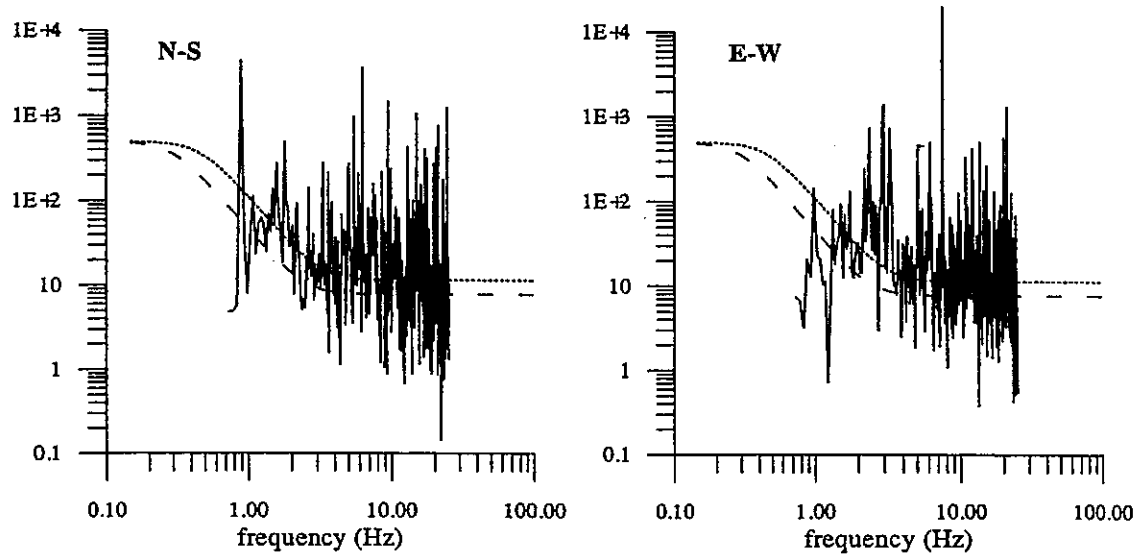

Figure 10. Comparison between the observed and calculated spectral ratios of mainshock (PAT11) and aftershock (PAT13). Solid line-observed data; dotted line-model of $R = 1.9$ km and $c = \frac{\Delta\sigma}{\Delta\sigma_a} = 2$; dashed line-model of $R = 3.0$ km and $c = \frac{\Delta\sigma}{\Delta\sigma_a} = 1$. The model curves were not fitted to the data, but independently found from EGF simulation.

source crustal structure the future source inversions in Western Greece will probably yield overestimated source radii, or will misinterpret simple ruptures as multiple events.

Acknowledgements

The authors thank G. Stavrakakis and I. Kalogeras (National Observatory of Athens) for providing the acceleration records, J. Jansky (Charles University) for modifying the crustal model by the ray method, and N. Melis (Patras University) for his advice. G.A. Ekström (Harvard University) provided extremely valuable comments. This work was supported by the EU Inco-Copernicus grants COME and ISMOD, the Czech Republic Grant Agency No. 205/1743, the Charles University Grant No. 5/97 and the Ministry of Education, Youth and Sports, Czech Republic, grants Nos. OK 278 and ME 060.

References

Bouchon, M., 1981, A simple method to calculate Green's functions for elastic layered media, *Bull. Seism. Soc. Am.* **71**, 959–971.

Coutant, O., 1989, Programme de simulation numerique AXITRA, *Rapport LGIT*, Universite Joseph Fourier, Grenoble.

Diagourtas, D., Makropoulos, K.C., Wajeman, C., Hatzfeld, D., Bard, P.-Y., Gariel, J.-C., 1994, Simulation of strong ground motion of the 14 July 1993 Patras earthquake and its contribution in the assessment of seismic hazard, Patras region, W. Greece. In: Makropoulos, C. and Suhadolc, P. (eds), *Proc. of ESC XXIV General Assembly*, Athens, Greece, 19–24 September 1994, pp. 1446–1454.

Ekström, G., Stein, R.S., Eaton, J.P. and Eberhart-Phillips, D., 1992, Seismicity and geometry of a 110-km-long blind thrust fault 1. The 1985 Kettleman Hills, California, Earthquake, *J. Geophys. Res.* **97**, 4843–4864.

Hutchings, L., 1994, Kinematic earthquake model and synthesized ground motion using empirical Green's function, *Bull. Seism. Soc. Am.* **84**, 1028–1050.

Irikura, K. and Kamae, K., 1994, Estimation of strong motion in broad-frequency band based on a seismic source scaling model and an empirical Green's function technique, *Annali di Geofisica* **XXXVII**, 1721–1743.

ITSAK, 1997, Bulletins of strong motion recordings of ITSAK strong motion network 1980–1994, ITSAK Internal Report, 97-01, 1997.

Kalogeras, I.S. and Stavrakakis, G.N., 1995, Analysis of Greek accelerograms recorded at stations of NOA's network time period 1990–1994, National Observatory of Athens (NOA), Geodynamic Institute, Publication No. 5.

Koukis, G., Tsiabaos, G. and Sabatakakis, G., 1997, Correlations of Mechanical Characteristics and Classification of Soil Units of Patras city. In: Atmatzidis, D. (ed.), *3rd Hellenic Conference on Geotechnical Engineering*, Patras, 20–22 March 1997, pp. 121–127.

Lindley, G.T., 1994, Source parameters of the 23 April 1992 Joshua Tree, California, earthquake, its largest foreshock, and aftershocks, *Bull. Seism. Soc. Am.* **84**, 1051–1057.

Makris, J., 1977, Geophysical investigations of the Hellenides, Hamburg Geophys. Einzelschriften, 34 Wittenborn; Hamburg, Reihe A.

Melis, N.S., Brooks, M. and Pearce, R.G., 1989, A microearthquake network in the Gulf of Patras, western Greece, and its seismotectonic interpretation, *Geophys. J. R. Astron. Soc.* **98**, 515–524.

Melis, N.S., Burton, P.W. and Brooks, M., 1995, Coseismic crustal deformation from microseismicity in the Patras area, *Geophys. J. Int.* **122**, 815–836.

Menke, W., 1984, Geophysical data analysis: Discrete inverse theory, Academic Press, Orlando, Florida.

Panagiotopoulos, D.G. and Papazachos, B.C., 1985, Travel times of P_n waves in the Aegean and surrounding area, *Geophys. J. R. Astron. Soc.* **80**, 165–176.

Pedotti, G., 1988. Etude sismotectonique du Peloponnese et reponse sismique d'une vallee sedimentaire en Grece du Nord, PhD Thesis, Université Joseph Fourier, Grenoble, 178 pp.

Plicka, V. and Zahradnik, J., 1998, Inverting seismograms of weak events for empirical Green's tensor derivatives, *Geophys. J. Int.* **132**, 471–478.

Stavrakakis, G.N., Kalogeras, I.S. and Drakopoulos, J.K., 1994, Analysis of accelerograms of the Patras' seismic sequence (14 July 1993) recorded at National Observatory of Athens (NOA) stations. In: Makropoulos, C. and Suhadolc, P. (eds), *Proc. of ESC XXIV General Assembly*, Athens, Greece, 19–24 September 1994, pp. 1455–1465.

Tselentis, G-A., Koukis, G., Sokos, E., Rubas, D., Jansky, J., Plicka, V., Pakzad, M. and Zahradnik, J., 1996, Modelling the strong ground motions in the city of Patras, Greece, during July 1993 earthquake. In: Sociedad Mexicana de Ingeniera Sismica (ed.), *Proc. 11th World conference on Earthquake Engineering*, Acapulco, Mexico 23–28 June 1996.

U.S. DEPT. OF INTERIOR/GEOL. SURVEY, 1993, Preliminary determination of epicentres. National Earthquake Information Center, Monthly Listing. July 1993.

Zednik, J., Jansky, J. and Cerveny, V., 1993, Synthetic seismograms in radially inhomogeneous media for ISOP applications. *Computers & Geosciences* **19**, 183–187.